Eng Int Syst (2023) 3: 205–213

Engineering
Intelligent Systems

Decision Tree Based Displacement Prediction Method of Laser Sensor

Lian Wu*

School of Electronic Engineering, Changzhou College of Information Technology, Changzhou 213164, China

To improve the fit between the displacement predicted results and the actual results, improve the measurement result accuracy, and improve the prediction efficiency, a laser sensor displacement prediction method on the basis of decision tree is put forward. In accordance with the operating principle of the laser sensor and the analysis results of the factors affecting the laser frequency (LF) stability, the precise relationship between the object and the image displacement is obtained; the decision tree is constructed, and the constructed decision number is used to mine the displacement data to improve the displacement prediction efficiency; on the basis of the displacement data mining results, the displacement comprehensive forecast index is calculated, and the value range of the displacement trend comprehensive forecast index is obtained through calculation. According to experimental results, the difference between the predicted results of the method in this paper and the actual displacement is small. The relative error of the predicted results is small, and the prediction efficiency is high. These results verify the application value of the method.

Keywords: decision tree; laser sensor; displacement prediction; comprehensive prediction index; phase space reconstruction

1. INTRODUCTION

As the science and technology and industrial technologies are constantly improved, the measurement industry has put forward higher and higher requirements for displacement prediction. Non-contact, high precision, high sensitivity, digitization and portability have become the main trends in the current development of the measurement industry [1]. Sensor technology is ubiquitous, laser sensors can ensure the accurate transmission of measured and predicted values [2, 3]. However, after a laser sensor has been used for a period of time or maintained, its technical indicators must be calibrated again to ensure that Its performance indicators still meet the requirements [4]. Today, with the increasing application scope and technical requirements, to further improve the displacement prediction effect, it is necessary to carry out improvement research on related technologies [5].

Li et al. [6] proposed a displacement prediction method on the basis of the LS-SVM model. Taking the Baishuihe landslide located in the area of the Three Gorges Reservoir as an example, the HP filter analysis method is used to extract the trend term of the landslide displacement (LD). The trend term displacement is mainly determined by the characteristics of the landslide itself. It has obvious nonlinear increasing characteristics, and polynomial is used for fitting and prediction. The periodic term is affected by a variety of inducing factors (landslide evolution stage, seasonal rainfall, reservoir water level rise and fall, etc.), and the least squares support vector machine model (LS-SVM) is used to train and predict it. The superposition of the combined predicted results is the cumulative displacement prediction value. The results show the prediction of monitoring points XD-04 and ZG93. Among them, the LS-SVM model has a high prediction level, and has good adaptability in the LD prediction with step-like displacement characteristics, but the obtained predicted value is different from the actual value. There is a certain deviation between the values. Yang et al. [7] proposed a displacement dynamic prediction model on the basis of long-short-term memory network and time series. The model first used the moving average method to brake up the landslide cumulative displacement into trend term displacement and periodic term displacement, and then used polynomial function for the prediction of the trend term. displacement. On the basis of the response analysis of the landslide deformation characteristics and inducing factors,

*Email of corresponding author: wulian7941085@126.com

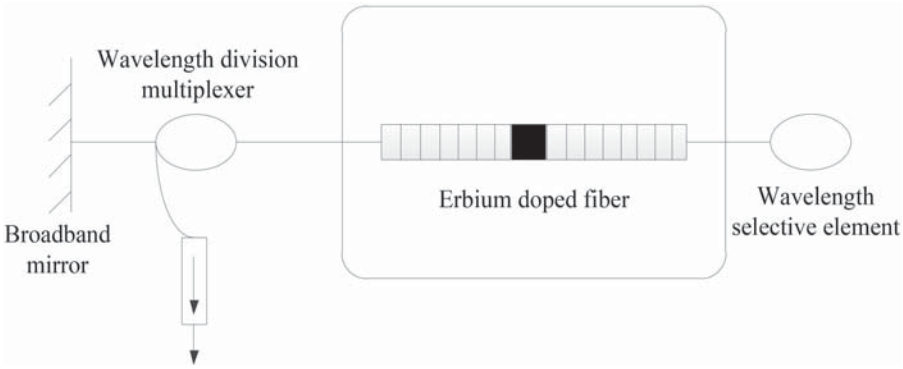

Figure 1 Operating principle diagram of laser sensor.

an LSTM model was established for the prediction of the periodic term displacement. Finally, the displacement of each sub-item is superimposed. In other words, the prediction of the cumulative displacement of the landslide is achieved. According to results, the prediction advantage of the method is particularly prominent in the step deformation period, and it does not depend on the training data, but the predicted results have large relative error. Li [8] proposed a method for predicting tunnel limit displacement on the basis of DE-GP collaborative optimization algorithm. Gaussian process was introduced into the calculation of tunnel limit displacement, and differential evolution algorithm was used instead of conjugate gradient method to search for the optimal value in the training process. To overcome the disadvantages of the conjugate gradient method over-reliance on the initial value, it is difficult to determine the number of iterations and local optimization, a limit displacement prediction method on the basis of the differential evolution-Gaussian process (DE-GP) collaborative optimization algorithm is formed. The generalization performance of a single kernel function Gaussian process is improved, and the solution process of limit displacement is greatly simplified. According to results, the generalization performance of the proposed method is good, but the prediction efficiency still needs to be improved.

To improve the fit between the predicted results of displacement and the actual results, reduce the relative error of the measurement results, and improve the prediction efficiency, a laser sensor displacement prediction method on the basis of decision tree is proposed.

2. DISPLACEMENT MEASUREMENT

2.1 Operating Principle of Laser Sensor

Laser sensor has very high sensitivity to external physical quantities such as temperature and strain. Using it as a displacement measurement tool not only has the advantages of ordinary sensors, but also can output higher signal-to-noise ratio and narrower bandwidth signals, which can achieve higher Resolution sensing. This paper takes the laser sensor as the research object, and mainly introduces the sensing principle of the laser sensor. The principle block diagram of the laser sensor is shown in Figure 1.

In accordance with Figure 1, the erbium-doped fiber (EDF) is placed between the wavelength selective element FBG and the broadband mirror, which together constitute the linear resonator of the laser sensor. The pump light is coupled into the EDF through a 980/1550 nm wavelength division multiplexer (WDM), and the EDF pumps it to generate a population inversion in the fiber, releasing photons around the 1550 nm wavelength to form spontaneous emission light. The spontaneous emission light is reflected multiple times between the FBG and the broadband mirror, so that the energy in the laser cavity is enhanced. When the gain in the laser cavity is greater than the transmission loss in the cavity, the laser can generate stable optical oscillation and output laser light.

In a laser cavity, for a resonator with a cavity length of L, to form a stable oscillation, its resonant frequency f_h is:

$$f_h = \frac{GT}{hL} \tag{1}$$

Among them, T represents the speed of light in vacuum; h represents the refractive index of medium in resonant cavity; G is an integer. For the oscillation satisfying Formula (1) to be excited, the threshold condition for laser generation must also be satisfied. Usually, a laser with only one frequency is called a single longitudinal mode laser. When the FBG bandwidth includes multiple mode intervals Δf_h, the laser works in a multi-longitudinal mode state, that is, a multi-longitudinal mode laser. where the pattern interval is:

$$\Delta f_h = \frac{\Delta L dz}{hL} \tag{2}$$

It can be known from Formula (2) that for resonant cavity sensing, the laser mode is determined by the refractive index and cavity length in the cavity.

In accordance with the different measured physical quantities, laser sensors can be divided into wavelength coding type and polarization type. Similar to the traditional sensor, the wavelength coded laser sensor measures the physical quantity through the change of the working wavelength of the laser. The change of the output wavelength can be detected in real time by the spectral analyzer (OSA) or by the unbalanced Mach Zehnder (M-Z) interferometer. Since the Bragg wavelength change of a laser sensor is a function of strain and temperature, wavelength-encoded laser sensors need to consider the elimination or compensation of the cross-sensitivity of strain and temperature to improve the accuracy

of the sensing system. The principle of the polarization state laser sensor is to write the FBG into the birefringent fiber. When the to-be-measured acts on the resonator, the birefringence of the fiber changes, which causes the beat frequency change between the two orthogonal polarization states of the output light. The resonant frequencies of the two orthogonal polarization modes (X-axis and Y-axis) are:

$$X = \int_{\infty}^{-\infty} \Delta h_x dz \tag{3}$$

$$Y = \int_{\infty}^{-\infty} \Delta h_y dz \tag{4}$$

Among them, Δh_x and Δh_y are the refractive indices of the two orthogonal polarization modes, respectively. The laser beat frequency $K(X, Y)$ caused by birefringence is:

$$K(X, Y) = \sum_{i=1}^{n} (x_i - y_i)^2 \tag{5}$$

Among them, x_i and y_i represent sensing primitives. When the sensor is far away from the light source, its output signal-to-noise ratio will be limited by the LF, which will affect the accurate sensing ability of the laser sensor. Therefore, to increase the displacement measurement level of the laser sensor, the factors that affect the stability of the LF are analyzed.

2.2 Factors that Affect the Stability of LF

For a laser sensor working in the fundamental mode, the oscillation frequency is:

$$f_k = f(x_j) \cdot V + E(\bar{h})L \tag{6}$$

Among them, x_j represents the order of the mode, which is a positive integer; V represents the speed of light in vacuum; $\bar{h}$ represents the average refractive index in the cavity. Formula (6) shows that the change of the cavity length L or the average refractive index $\bar{h}$ will lead to the change of laser oscillation frequency. The change formula is:

$$\Delta f_k = \omega_i \times \left(\frac{\Delta L}{h} + \frac{\Delta L}{\bar{h}} \right) \times r_{ij} \tag{7}$$

Among them, ω_i represents the medium frequency; r_{ij} represents the decay rate of the oscillation.

Therefore, the stabilization of the LF can be attributed to the problem of maintaining the cavity length and refractive index stable, and the external factors affecting the frequency stability basically include the following aspects:

(1) Influence of temperature changes

Due to the fluctuation of ambient temperature or the heating of the laser during operation, the cavity length will expand and contract with the change of temperature, resulting in frequency drift. Since the temperature generally changes slowly, the temperature mainly affects the long-term stability of the frequency. The relative change relationship between cavity length and frequency due to temperature change is:

$$\Delta T = \frac{(\delta - 1)\Delta L}{\Delta \eta} \tag{8}$$

Among them, ΔT represents the temperature change; δ represents the linear expansion coefficient of the cavity spacer material; $\Delta \eta$ represents the center wavelength change.

Thermostatically control the entire laser system to minimize the effects of temperature changes.

(2) The influence of atmospheric changes

For external cavity and semi-external cavity lasers, the resonant cavity's length is L and the discharge tube's length is L_1, then the relative length of the part which is exposed to the atmosphere is $(L - L_1)L$. Changes in atmospheric temperature, humidity and air pressure will cause changes in the atmospheric refractive index. As a result, the laser's oscillation frequency is fluctuated.

(3) Influence of magnetic field

To reduce the influence of temperature, the spacer of the laser resonator is mostly made of invar material. However, the magneto strictive properties of invar may cause the change of the cavity length, so the effect of the geomagnetic field and the stray magnetic field of the electronic instruments around the laser have a negative impact on the highly stable laser. Or the effect of frequency stabilized lasers by magnetic field effects must be considered.

The above points are external factors that cause frequency instability. In addition, due to changes in the laser's discharge current and air pressure, as well as internal factors such as random noise caused by spontaneous radiation, the frequency stability can also be affected. It is controlled by the pressure device, which cannot be totally controlled, so it is an intrinsic factor limiting the stability of the LF.

2.3 The Exact Relationship Between Object-Image Displacement

In addition to the influencing factors analyzed in Section 2.2, the incident light spot moves as the workpiece deviates from the imaging optical axis, and its image point must also deviate from the optical axis, therefore, it will also affect the displacement measurement results. To maintain the image point on the light receiver always on the focal plane, the light receiver's light-receiving surface must form an included angle β with the imaging optical axis. The purpose is to establish the precise relationship between the incident light spot and the displacement of the image spot in accordance with the imaging principle, and to minimize the image spot, which is beneficial to improve the measurement accuracy. Figure 2 is a diagram of the incident light spot and the displacement trajectory of its image point under the conditions mentioned above.

In Figure 2, d_1 and d_2 are the displacements of the incident light spot and its image point, respectively. When the incident light spot moves from point a to point b with the measured

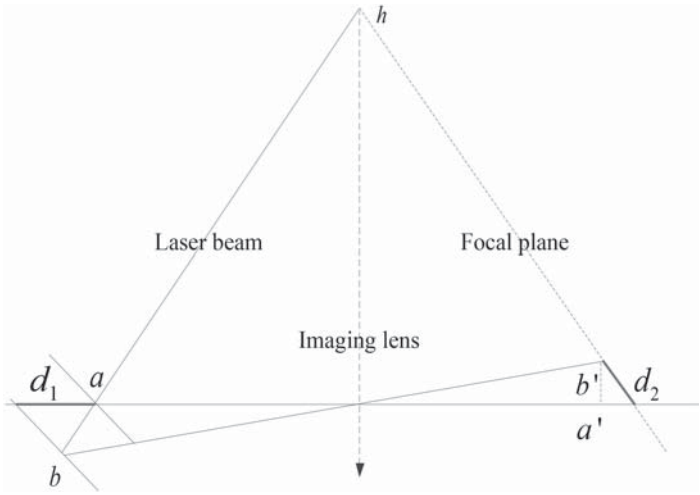

Figure 2 Object-image displacement trajectory diagram.

object surface, the image point b', based on the imaging principle, is obtained. Besides, the extension $a'b'$ intersects with the laser beam at point h, thus:

$$ba_1 = d_1 \cos 0 \tag{9}$$

$$b'a'_1 = d_2 \sin \phi \tag{10}$$

In accordance with the similar principle, we get:

$$d_1 = \frac{d_2 \nu_1 \cos \phi}{\nu_1 \cos 0 - d_2 \cos \phi} \tag{11}$$

$$d_2 = \frac{d_1 \nu_1 \sin \phi}{\nu_1 \sin 0 + d_1 \sin \phi} \tag{12}$$

The above formula shows that the incident light spot is transferred with the surface of the object to be measured, and the precise relationship of the change of the image point can be determined in accordance with the transfer direction, thereby realizing the displacement measurement by using the laser sensor.

3. DISPLACEMENT PREDICTION METHOD

On the basis of the measurement results of the laser sensor displacement obtained in Section 2, the decision tree algorithm (DTA) is further used to predict the displacement.

3.1 Displacement Data Mining

3.1.1 Decision Tree Generation

The decision tree refers to a tree structure similar to a flowchart, in which the internal node of the tree indicates a test of an attribute (value). And its branches indicate each result of the test [9]. To identify and categorize unknown data objects, the attribute values which are in the data set can be tested in accordance with the decision tree structure. A path starting from the root node of the decision tree and ending at the leaf node forms the corresponding object's category prediction [10]. In addition, compared with many algorithms that can also realize classification prediction, the biggest feature of DTA is that its classification prediction is on the basis of logic, that is, the classification prediction of output variables is realized through the logical comparison (Boolean comparison) of the values of input variables.

The recursive DTA is used to construct the top-down decision tree. With the uninterrupted deep-seated construction of the decision tree, the training sample set will be recursively decomposed into several smaller subsets [11]. The path between the tree root and each node corresponds to an association rule. Therefore, the whole decision tree is in correspondence with a complete set of association rules. The generation process of decision tree algorithm is shown in Figure 3.

3.1.2 Displacement Data Mining on the Basis of Decision Tree

With the continuous improvement of multi-source information acquisition methods, communication technology, network technology and other technologies are further improved and improved, the data in various databases has increased dramatically, and the content covered has become more complex and huge. The traditional data processing technology has been unable to effectively deal with the increasing amount of data, and the important regular knowledge hidden in it is waiting for people to use new and more effective technology to realize mining. Data mining technology provides a way to deal with this problem [12]. At present, data mining technology is adopted for the analysis of the displacement monitoring data, and excavate the data that is beneficial to the displacement prediction.

A classification model is most effectively represented by a decision tree. Among them, each internal node of the tree indicates a test on an attribute. Each branch indicates a test output. Each leaf node indicates a class or class distribution. During tree construction (induction), pruning is required for detecting and removing noise and outliers in the training data, thereby improving the accuracy of unknown data classification.

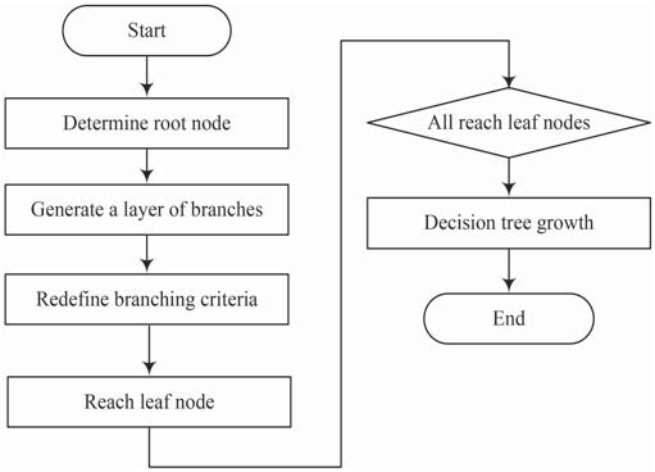

Figure 3 Flowchart of decision tree algorithm generation.

In the DTA, S_x is a known training sample, and S_y is a candidate attribute set. The information gain entropy I_e^2 is used to select each node of the tree, which is called branch optimization. The expression of I_e^2 is:

$$I_e^2 = \sqrt{S_x + S_y} \times \left[\sigma(Q_i) + \sigma(Q_j)\right] \tag{13}$$

Among them, σ represents the associativity function; Q_i and Q_j represent the adjacent layers in the spanning tree.

The attribute (column) with the highest information gain (maximum entropy) is selected as the current node's judgment (decision) attribute [13]. The amount of information necessary for sample classification in the resulting division is minimized by this attribute and the minimum randomness of the division is reflected. Based on this, a relatively simple tree can be constructed to achieve the purpose of improving the efficiency of displacement prediction.

Let U be a set of m displacement data samples, assuming that there are M distinct values in class label attribute, and M distinct classes V_i is defined, where $i = 1, 2, \ldots, M$. Let U_i be the number of samples in class V_i, the expected value required for classifying a given sample is obtained by:

$$I(u_1, u_2 \ldots, u_m) = \log_2 W_i \times (u_{ki} + u_{kj}) \tag{14}$$

Among them, W_i represents the probability of any sample belonging to class V_i; u_{ki} and u_{kj} both represent the attribute contribution of the sample.

Suppose attribute R has g different values $\{s_1, s_2, \ldots, s_g\}$, and attribute R is used to divide U into g subsets $\{U_1, U_2, \ldots, U_g\}$. With the value r_i on the attribute R, if R is chosen as the attribute of judgment, then these subsets are corresponding to the branches grown from the nodes containing the set U.

Let U_{ij} be the number of samples of class V_i in subset U_i. The entropy decomposed into subsets in accordance with R is expressed by Formula (15):

$$B_i = \sum_{i=1}^{m} D_i(w_i) \times U_i \tag{15}$$

The smaller entropy value will lead to the higher subset division accuracy. In accordance with the result of the subset division, the required sample data can be selected, that is, the displacement data mining is completed.

3.2 Comprehensive Forecast Index

Taking the displacement data mining results as the data basis, to realize the prediction of the displacement, the displacement comprehensive prediction index is firstly calculated. When predicting the displacement trend, it is mostly the effect of the combined superposition of various factors on the displacement, and this superposition combination is diverse, and the predicted result on the basis of only one of the criteria is not accurate enough. On the basis of the category attribute values obtained when constructing the decision tree model in Section 3.1.2, this paper divides all factors into four categories, assigns the same weight to the same category of each factor, and takes the importance of each factor as the feature of each factor weights, and then superimpose the weights of each factor to determine a comprehensive forecast index:

$$K_z = \sqrt{\sum_{i=1}^{n} F_z \times C_z} \tag{16}$$

Among them, F_z represents the importance of each factor variable; C_z represents the weight of each category.

In accordance with the above analysis, the constructed decision tree model is used to divide each factor into different categories, and assign weights to each category to obtain comprehensive forecast criterion information. The value range of the displacement trend comprehensive forecast index is obtained by calculation, and the displacement trend can be qualitatively or quantitatively predicted by using this index.

3.3 Displacement Prediction on the Basis of Phase Space Reconstruction

3.3.1 Phase Space Reconstruction

According to the research of chaotic dynamics, the time series of any variable determining the long-term evolution of the

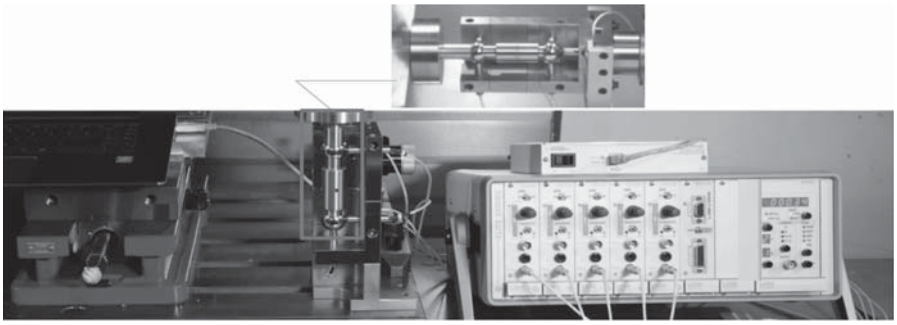

Figure 4 Physical map of the laser sensor.

system contains the information of the long-term evolution of all variables of the system [14]. Therefore, the system's long-term evolution information can be recovered and extracted from any univariate time series determining the system's long-term evolution and containing all the variable traces of the system's participation in motion. The complex feature of time series is the result of the evolution of a specific trajectory (chaotic attractor) generated by a chaotic system after similar stretching and folding [15].

In the displacement prediction, let the univariate displacement time series be $T(t_i)$, and its sampling time interval be ΔT. Then the reconstructed phase space is:

$$X[T(t_i)] = \frac{\alpha_1 t^2}{e^{\alpha_2/t^2} - 1} \times \Delta T \tag{17}$$

Among them, α_1 and α_2 represent the embedding dimension; t^2 represents the delay time.

Call $X[T(t_i)]$ the phase point in the k-dimensional phase space, and N the number of phase points:

$$N = \frac{\varepsilon(m-1)}{X[T(t_i)]} \tag{18}$$

Among them, ε is used to describe the evolution trajectory of the phase space. In accordance with Takens' embedding theorem, as long as the choice is appropriate, the "trajectory" of the phase space reconstructed in the embedding space is the "dynamic equivalence" of the original system in the topological sense. Its dynamic properties, such as Lyapunov exponent and fractal dimension, can remain unchanged.

In accordance with the embedding theorem, for a proper ε, there exists a smooth map $y{:}P^{\varepsilon} \rightarrow P^{\varepsilon}$ such that:

$$X[T(t_i + 1)] = yX[T(t_1)] \tag{19}$$

Theoretically, y that satisfies the above formula is unique, but in practical applications, because the data in hand is always limited, it is impossible to obtain y, and only the mapping $\overline{y}$: $P^{\varepsilon} \rightarrow P^{\varepsilon}$ can be constructed from the limited observation data, so that $\overline{y}$ is sufficiently close to y.

The local method is one of the methods of constructing $\overline{y}$. It takes the last point of the phase space trajectory as the center point, finds the phase points adjacent to the center point, and then performs fitting from these reference points. The first-order approximation is the most commonly used in the local method, and the phase space trajectory is assumed to satisfy in a certain neighborhood of the center point $X[T(t_n)]$:

$$X[T(t_n + 1)] = \theta + \eta X[T(t_n)] \tag{20}$$

If there are j reference points in the neighborhood, use the least squares method to obtain θ and η, and then the prediction expression can be obtained.

The distance between each point in the phase space and the center point is a very important parameter, and the accuracy of the prediction often depends on the points closest to the center point in space. Therefore, introducing the spatial distance as a fitting parameter into the prediction process can increase the prediction accuracy to a certain extent and has a certain ability to eliminate noise. The prediction of its phase space trajectory can be described as:

$$X[T(t_n + N)] = \frac{1}{\sqrt{|B_r|}} - \sum_{i=1}^{N} e^i \times e^j \tag{21}$$

Among them, B_r represents the predicted trajectory point; e^i and e^j represent each point in the neighborhood of the center point; B_r is an adjustable parameter, and by adjusting B_r, the prediction mode can be better adapted to different data, and $B_r \geq 1$ is generally taken. If the first $(m-1)$ dimension of $X[T(t_n+N)]$ is known, the last dimension of $X[T(t_n+N)]$ is obtained, which is the obtained displacement prediction value.

4. EXPERIMENTAL VERIFICATION

To verify the validity of the laser sensor displacement prediction method on the basis of decision tree, experiments are carried out. The experiment in this paper adopts the form of comparison. The displacement prediction method on the basis of the LS-SVM model and the displacement dynamic prediction model on the basis of the long-short-term memory network and the time series are used as comparison methods to compare with the method in this paper.

4.1 Experimental Equipment

In the experiment, the selected displacement measurement laser sensor is VE—521/VT—510 capacitive displacement sensor produced by ON-OSOKKI company of Japan, with a measurement range of 0.5 mm/5 V and a resolution of 100 nm. Figure 4 shows the physical diagram of the laser sensor used in the experiment, and Table 1 shows the specific parameter indexes of the laser sensor.

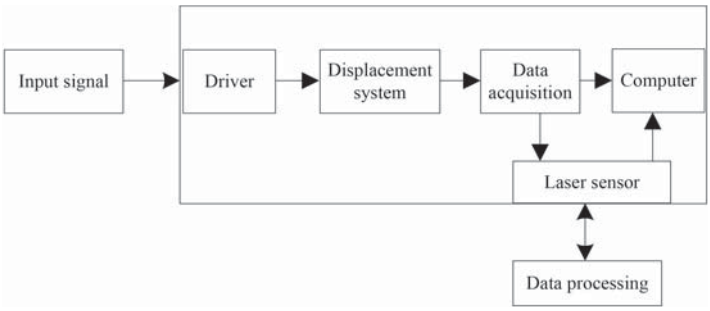

Figure 5 Calibration principle diagram of displacement simulation system.

Table 1 Laser sensor parameters.

Index	Parameter
Response time	1um
Output type	NPN normally closed contact (NC)
Operating temperature	80 °C
Voltage	12 V
Spot diameter	25 μm

4.2 Experimental Principle and Steps

A displacement simulation system is established. The principle of the system generating micro-displacement is: when the voltage signal flows through the piezoelectric driver, the two ends of the piezoelectric driver are polarized to form an external electric field, which causes the piezoelectric driver to simultaneously generate inverse piezoelectric effect and electric field. The deformation occurs due to the stretching effect, and the magnitude of these deformations is the displacement generated in this experiment. The displacement system used in this paper belongs to a micro-displacement generating device, which is convenient for the laser sensor to accurately measure its displacement, which makes the experimental results more accurate and credible. Figure 5 is the calibration principle diagram of the displacement simulation system.

Build a calibration test bench in accordance with the experimental device, transmit the generated signal to the driver, and the driver will drive the displacement system to generate tiny displacements. Install the laser sensors at both ends of the displacement system, collect the displacement generated by the displacement system, and record and save the experimental results.

4.3 Experimental Results

(1) Fitting analysis between predicted value and actual value

To verify the effect of displacement prediction, the fit which is between the actual value and the predicted value is used as the evaluation index. A higher fit between the two leads to a better prediction effect of the method. Table 2 shows the comparison results of different methods.

Seen from the data in Table 2, the difference between the displacement predicted by the method in this paper and the actual displacement is small, and the error interval is between [1–0.03]. In the seventh experiment, even with the actual predicted values are completely coincident, indicating that the predicted results of the proposed method have a good fit with the actual results, that is, the prediction effect of the proposed method is better. However, the displacement prediction method on the basis of the LS-SVM model and the displacement dynamic prediction model on the basis of the long-short-term memory network and the time series have a large gap between the predicted value and the actual value, that is, the fit between the actual predicted value is poor, the prediction effect is not good.

From the above comparison, it can be seen that the prediction effect of the method in this paper is better. To express it more intuitively, the predicted result is drawn as an image, and the prediction trend curve is shown in Figure 6.

Observing Figure 6, it can be seen that the degree of coincidence between the actual value of the proposed method and the predicted value is large, that is, the fitting between the two is good, which further verifies the prediction effect of the proposed method.

(2) Comparison of relative errors of predicted results

The relative error of the predicted result is used as the evaluation index, and the displacement prediction effect of different methods is compared. The calculation formula of the relative error is as follows:

$$E_r = \frac{\lambda_i}{\lambda_j} \times 100\% \tag{22}$$

Among them, λ_i represents the probability that the displacement is correctly predicted; λ_j represents the probability that the displacement is wrongly predicted. The relative error results of the predicted results obtained by different methods in accordance with Formula (22) are shown in Figure 7.

In accordance with Figure 7, the relative error of the predicted results of the proposed method is low, which is lower than that of the LS-SVM model and the method on the basis of long-short-term memory network and time series in many experiments. The relative error is always lower than 0.3. The relative error of the model and the method on the basis of long-short-term memory network and time series is large, and there is a certain volatility. It can be found that the predicted results of this method are more accurate.

(3) Comparison of prediction efficiency

Table 2 Fits between predicted and actual values.

Number of experiments/time	Displacement/cm			
	Actual value	The method of this paper	LS-SVM model	Time series and long short-term memory networks
1	3.57	3.56	3.79	3.20
2	4.02	4.01	4.15	3.53
3	4.26	4.24	4.39	4.11
4	− 0.12	− 0.14	− 0.21	− 0.07
5	− 0.50	− 0.47	− 0.39	− 0.37
6	6.32	6.31	6.25	6.57
7	6.79	6.79	6.53	6.82
8	3.27	3.25	3.72	3.26
9	− 0.10	− 0.13	− 0.19	− 0.09
10	− 0.19	− 0.18	− 0.24	− 0.18

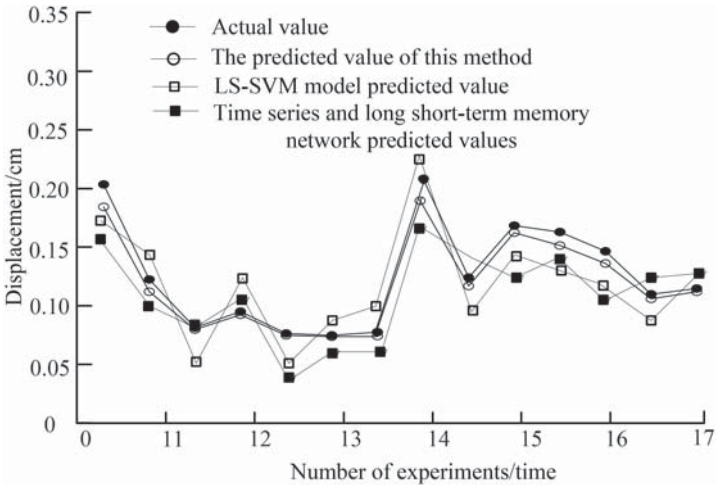

Figure 6 Predicted trend curve.

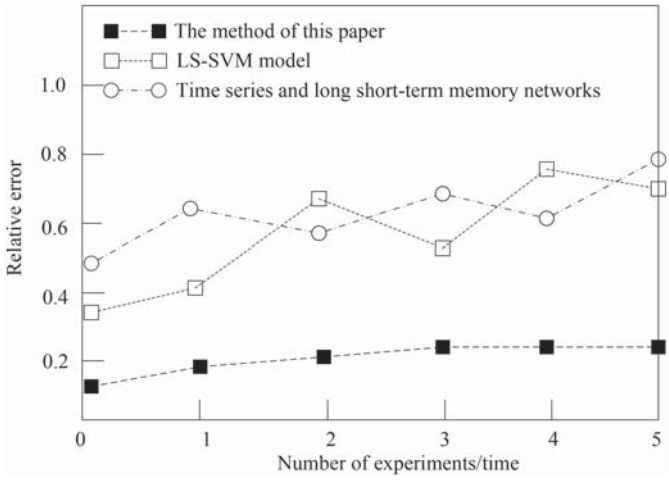

Figure 7 Relative error comparison results of predicted results.

To further verify the prediction efficiency of the proposed method, the comparison results of the prediction time of different methods are presented in Table 3.

According to the analysis of the data in Table 3, the increase of the number of experiments leads to the increase of the prediction time of different methods. When the number of experiments is 2, the prediction time of the method in this paper is 2.1 s, the prediction time of the LS-SVM model is 6.8 s, and the prediction time of the long-short-term memory network and the time series method is 9.4 s. It can be seen that compared with the LS-SVM model and the long-short-term memory network and time series methods, the prediction

Table 3 Comparison results of prediction efficiency of different methods /s.

Number of experiments/time	The method of this paper	LS-SVM model	Long short-term memory networks and time series
1	1.9	4.8	6.1
2	2.1	6.8	9.4
3	3.5	8.3	11.6
4	3.7	10.7	14.8
5	4.0	13.5	17.5

time of the method in this paper is shorter, indicating that its prediction efficiency is higher.

5. CONCLUSION

To improve the fitting degree between the displacement predicted results and the actual results, the measurement result accuracy and the prediction efficiency, a displacement prediction method of laser sensor on the basis of decision tree is put forward. The operating principle of laser sensor and the factors affecting the stability of LF are analyzed, and the accurate relationship between object image displacement is obtained; Establish a decision tree to mine displacement data and improve the efficiency of displacement prediction; On the basis of the displacement data mining results, the displacement comprehensive prediction index is calculated, and the value range of the displacement trend comprehensive prediction index is obtained through calculation. At the same time, the phase space reconstruction is performed to realize the displacement prediction. Experimental results suggest a small gap between the predicted results and the actual displacement, a small relative error of the predicted results, and a high prediction efficiency, which verifies the application value of this method.

REFERENCES

1. D'Emilia, G., Gaspari, A., Natale, E., Adduce, G., Vecchiarelli, S. (2021). All-around approach for reliability of measurement data in the industry 4.0. IEEE Instrumentation and Measurement Magazine, 24(1), 30–37.
2. Gaol, FL., Matsuo, T. (2020). The simulation of implications of sensor technology on the new product development to solve lot-sizing problems with fuzzy approach. Journal of Sensors, 2020(3), 1–15.
3. Sward, KA., Dabbs, DV. (2020). The expanding science of sensor technology in research. Nursing Outlook, 68(6), 689–692.
4. Fukuda, D. (2019). Single-photon measurement techniques with a superconducting transition edge sensor. IEICE Transactions on Electronics, 102(3), 230–234.
5. Gauthier, A., Pruvost, M., Gamache, O., Colin, A. (2021). A new pressure sensor array for normal stress measurement in complex fluids. Journal of Rheology, 65(4), 583–594.
6. Li, SB., Li, DY., Zhang, YE., Li, J. (2019). Displacement prediction of Baishuihe step-like landslide by least square support vector machine. Journal of Yangtze River Scientific Research Institute, 36(4), 55–59+76.
7. Yang, BB., Yin KL., Du J. (2018). A model for predicting landslide displacement based on time series and long and short term memory neural network. Chinese Journal of Rock Mechanics and Engineering, 37(10), 2334–2343.
8. Li, XS. (2021). Prediction of tunnel limit displacement based on DE-GP collaborative optimization algorithm. Modern Tunnelling Technology, 58(2), 78–85.
9. Almeida, R., Neto, W., Silva, V., Carvalho, L., Gomes, R. (2021). Decision tree as a tool in the classification of lima bean accessions. Revista Caatinga, 34(2), 471–478.
10. Hoang, T., Nguyen, VD., Van, AD., Nguyen, H. (2020). Decision tree techniques to assess the role of daily DO variation in classifying shallow eutrophicated lakes in Hanoi, Vietnam. Water Quality Research Journal of Canada, 55(1), 67–78.
11. Milkov, AV., Samis, JM. (2020). Turning dry holes from disasters to exploration wisdom: Decision tree to determine the key failure mode for segments in conventional petroleum prospects. AAPG Bulletin, 104(2), 449–475.
12. Bardak, S., Bardak, T., Peker, H., Szen, E., Abuk, Y. (2021). Predicting effects of selected impregnation processes on the observed bending strength of wood, with use of data mining models. Bioresources, 16(3), 4891–4904.
13. Wei, P., Shi, C., He, F. (2020). Simulation on static detection of malicious code based on behavior information gain. Journal of Intelligent and Fuzzy Systems, 38(6), 1–10.
14. Xing, HY., Liu, G. Simulation research on chaotic system space reconstruction parameters. Computer Simulation, 35(7), 212–216.
15. Sagheer, A., Kotb, M. (2019). Time series forecasting of petroleum production using deep LSTM recurrent networks. Neurocomputing, 323(5), 203–213.